Journal of Solid State Chemistry 183 (2010) 720–726

Contents lists available at ScienceDirect

Journal of Solid State Chemistry

journal homepage: www.elsevier.com/locate/jssc

Structural and physical properties evolution of $BaIr_{1-x}Mn_xO_3$ solid solutions synthesized by high-pressure sintering

J.G. Zhao [a,b], L.X. Yang [a], Y. Yu [a], F.Y. Li [a], R.C. Yu [a], C.Q. Jin [a,*]

[a] Beijing National Lab for Condensed Matter Physics, Institute of Physics, Chinese Academy of Sciences, Beijing 100190, PR China
[b] Natural Science Research Center, Academy of Fundamental and Interdisciplinary Sciences, Harbin Institute of Technology, Harbin 150080, PR China

ARTICLE INFO

Article history:
Received 3 September 2009
Received in revised form
18 January 2010
Accepted 20 January 2010
Available online 28 January 2010

Keywords:
High-pressure synthesis
Hexagonal perovskite
B-site solid solutions
Magnetic property
Electrical conductivity

ABSTRACT

The $BaIr_{1-x}Mn_xO_3$ ($0.0 \le x \le 1.0$) solid solutions were synthesized by using the solid-state chemical method and high pressure sintering in the pressure range 0–5 GPa. According to the pressure–composition "phase diagram" at 1000 °C, the 9M $BaIr_{1-x}Mn_xO_3$ transforms to the 6M form at 5 GPa and $x \le 1/6$. In the x range 0.5–1.0, it transforms to the 9R form in a large pressure range. For the 9M $BaIrO_3$, the Mn ions substitution for Ir ions enhances the semiconducting property, and reduces the weak ferromagnetism. When x is larger than 1/3, the 9M/9R $BaIr_{1-x}Mn_xO_3$ behave spin–glass-like state at low temperature, with the glass transition temperature T_g about 60 K. For the 6M $BaIrO_3$, the Mn ions doping results in that it transforms to insulator and spin–glass-like magnetism from the initial paramagnetic metal.

1. Introduction

At ambient pressure, $BaIrO_3$ crystallizes into the monoclinic structure, with the space group $C2/m$, rather than the rhombohedral structure [1]. The ion coordination of $BaIrO_3$ is similar with that of the 9R $BaRuO_3$, so it is denoted to 9M. It is the first known ferromagnet that contains a 5*d* transition metal cation in the ternary oxides, with the Curie temperature T_c about 183 K [2]. The weak ferromagnetism originates from spin polarization of Ir cations rather than from spin canting [3–5]. By treating the 9M $BaIrO_3$ with high-temperature and high-pressure method, we obtained the 6M $BaIrO_3$ at 5 GPa and 1000 °C [6]. The structure of the 6M $BaIrO_3$ is similar with that of the ambient-pressure phase of $SrIrO_3$ with the space group $C2/c$ [7]. Recently, Cheng et al. found that one new form of $BaIrO_3$, which is treated at 3.3–4.0 GPa and 1000 °C, adapts a 5-layer structure, with the space group $C2/m$ [8]. We denoted this new intervenient polymorph of $BaIrO_3$ between the 9M and 6M forms as 5M. The 9M $BaIrO_3$ is a semiconductor for the polycrystal sample [9], but the 6M form is a paramagnetic metal [6]. The 5M $BaIrO_3$ is a weak ferromagnetic metal according to our recent results [10].

It is easy to obtain the 6M or 6H $Ba_3MIr_2O_9$ at ambient pressure by substituting 1/3 *M* cations (*M*=alkali metals, alkaline earth elements, 3*d* transition metals, and lanthanides) for Ir ions in $BaIrO_3$ [11–13]. In these compounds, the *M* and Ir ions occupy the corner-sharing octahedrons sites (in the MO_6 octahedron) and the face-sharing octahedrons sites (in the Ir_2O_9 dioctahedron), respectively. The chemical substitution results in the change of physical properties. All these compounds with Ir-site substitution are semiconducting, although there is the unpaired *d* or *f* electron in most *M* cations [11–13]. Their magnetic properties are very complex, containing the contributions of *M* cations and Ir–Ir direct interaction.

At ambient condition, $BaMnO_3$ adopts the 2H form, which contains chains of face-sharing octahedrons parallel to *c*-axis [14,15]. Under high pressure and high temperature, the 2H $BaMnO_3$ can transform to the 9R and 4H forms [16], which is similar with that in $BaRuO_3$ [17]. Considering the similar structure and pressure behavior, $BaIr_{1-x}Mn_xO_3$ will transform to the other normal or distorted hexagonal perovskite structures from the initial 9M or 2H forms under sufficient high synthesis pressure. Fig. 1 shows the schematic views of the 9M, 5M, 6M, 9R, 4H, and 2H forms of $BaIr_{1-x}Mn_xO_3$.

$BaIr_{1-x}Mn_xO_3$ at x=0.58 has been synthesized at ambient pressure and it adopts the 9R form [18]. However, the structural evolution and physical properties of these serial compounds have not been obtained, and the high-pressure phases have not been investigated so far. In this paper, we synthesized $BaIr_{1-x}Mn_xO_3$ using solid state chemical method and high-pressure sintering, and reported the structural, electrical and magnetic properties of the 9M/9R series and 6M series.

* Corresponding author at: Beijing National Lab for Condensed Matter Physics, Institute of Physics, Chinese Academy of Sciences, Beijing 100190, PR China.
Fax: +86 10 82640223.
E-mail address: zhaojinggeng@163.com (C.Q. Jin).

0022-4596/$ - see front matter © 2010 Elsevier Inc. All rights reserved.
doi:10.1016/j.jssc.2010.01.019

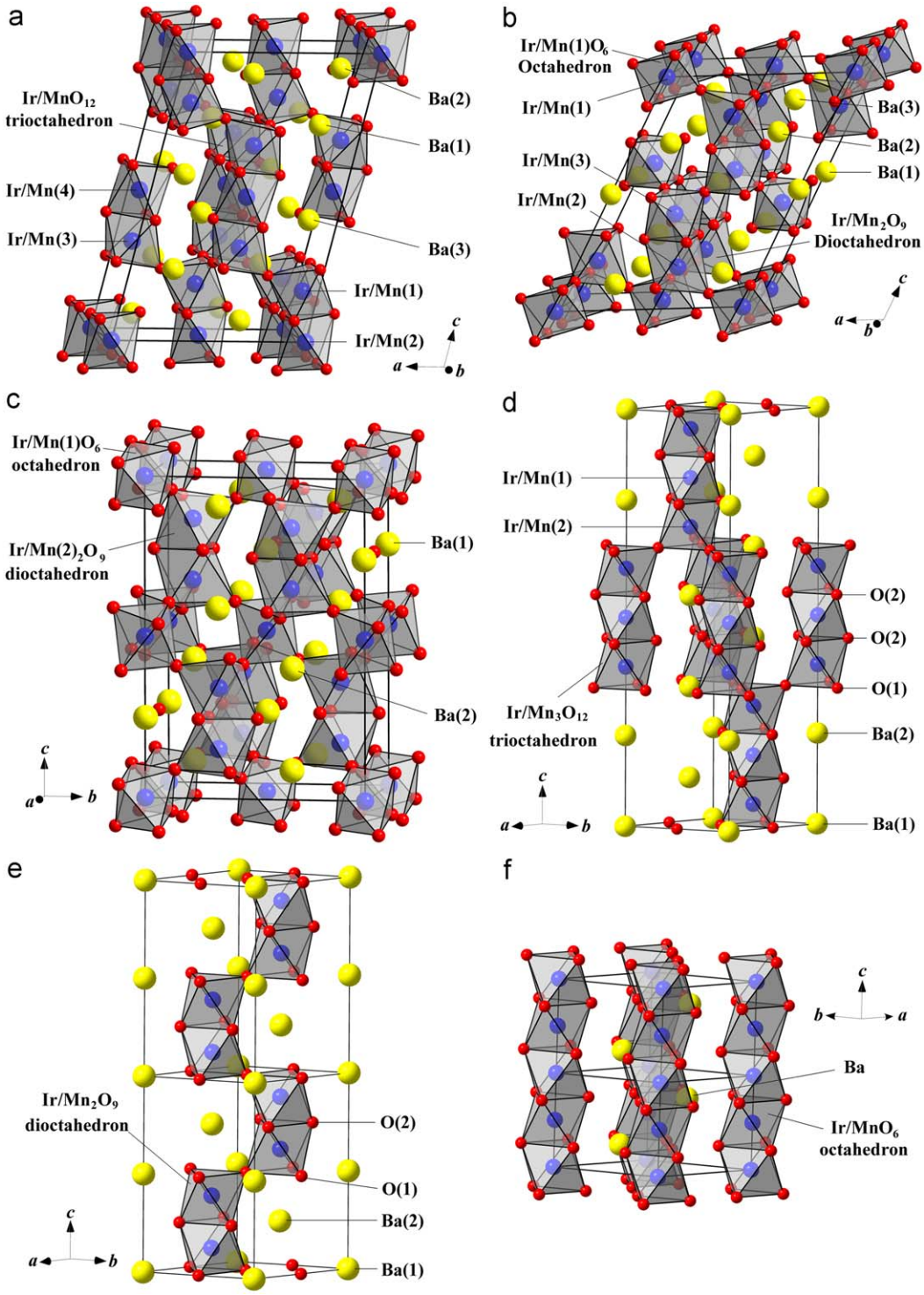

Fig. 1. The schematic views of the four crystallographic forms of $BaIr_{1-x}Mn_xO_3$: (a) 9M form; (b) 5M form; (c) 6M form; (d) 9R form; (e) 4H form; and (f) 2H form. The Ir/MnO_6 octahedrons are represented by geometrical coordination (Ir/Mn at the center, O at corners). The unit cells are outlined.

2. Experiment

The ambient phases of $BaIr_{1-x}Mn_xO_3$ were synthesized by using the method of conventional solid state chemical reaction. The starting materials were barium carbonate (99.9% purity), iridium metal (99.9% purity), and Mn_2O_3 (99.9% purity). Stoichiometric quantities of materials were mixed together, ground about 30 min in an agate mortar, and placed into an Al_2O_3 crucible. Then the powder was calcined for about 12 h at 900 °C in air. The calcined powder was reground, pressed into a pellet at the pressure of 10 MPa, and sintered at 1000 °C for about 72 h in air with twice intermediate regrinding.

A conventional cubic-anvil type high-pressure facility was used to perform the high-pressure and high-temperature experiments. The ambient $BaIr_{1-x}Mn_xO_3$ were pressed into pellets of 5.0 mm diameter, and then wrapped with gold foil to avoid contamination. The pellets were put into an h-BN sleeve which was in turn inserted into a graphite tube heater. Pyrophyllite was

used as the pressure-transmitting medium. The treating process was carried out at 1.5–5.0 GPa and 1000 °C for about 30 min, followed by a quench from high temperature before releasing pressure.

The structures of our samples were checked by the powder X-ray diffraction (XRD) with Cu$K\alpha$ radiation at room temperature, using a Rigaku diffractometer (MXP-AHP18). The measurements of temperature dependences of electrical resistivity were performed by using the standard four-probe method with Ag paste contacts on an Oxford Maglab measuring system in the temperature range of 2–300 K. The relationships of magnetic susceptibility versus temperature were obtained by using a SQUID magnetometer (Quantum Design, MPMS-5S) in the temperature range of 5–300 K. Data were collected under both zero-field-cooled (ZFC) and field-cooled (FC) conditions in the applied field of 0.1–1 T.

3. Results and discussion

3.1. Crystal structure

Fig. 2 shows the "phase diagram" at 1000 °C, which summarizes the results of $BaIr_{1-x}Mn_xO_3$ as a function of pressure and composition. The dashed line is not the strict borderline between the two neighboring phases. The arrangement of Ir and Mn cations is disordered with Mn substituted randomly for Ir cations, due to the comparable radius of Mn and Ir cations [19]. At ambient pressure, $BaIr_{1-x}Mn_xO_3$ crystallizes into the 9M form at $x \leq 1/3$ and transforms to the 9R form when x is larger than 1/3. It adopts the 2H form when x is equal to 1.0, i.e. $BaMnO_3$. High-pressure sintering changes the structure of $BaIr_{1-x}Mn_xO_3$ to the new forms. At 5 GPa, $BaIr_{1-x}Mn_xO_3$ adopts the 6M form at $x \leq 1/6$. As shown in Fig. 2, at 4 GPa and x=0.0–1/6, and at 5 GPa and x=1/3, there are the 5M phases in the "phase diagram". Fig. 3(a) shows the XRD patterns of the 9M, 6M and 5M $BaIr_{0.95}Mn_{0.05}O_3$. At 5 GPa and x=0.5, $BaIr_{1-x}Mn_xO_3$ crystals into the 4H form. When x is larger than 0.5, $BaIr_{1-x}Mn_xO_3$ mainly adopts the 9R form, and there is a mixed region between the 9R and 4H forms. There is also a mixed region between the 9R and 2H forms in the "phase diagram". Fig. 3(b) shows the XRD patterns of the 2H, 9R, and 4H forms of $BaIr_{1-x}Mn_xO_3$ with different Mn content.

Fig. 3(c and d) shows the XRD patterns of the 9M/9R and 6M $BaIr_{1-x}Mn_xO_3$, respectively. The lattice parameters are calculated from Le Bail refinements. Fig. 4(a and b) shows the relationships of the volume of one chemical formula unit V_N and normalized lattice parameter a_N, b_N, and c_N, and β versus the Mn content x for the 9M/9R and 6M $BaIr_{1-x}Mn_xO_3$, respectively. The insets of (a) and (b) show the x dependence of β for the 9M and 6M forms, respectively. $V_N = V/n$, where n is equal to 9 and 12 for the 9R and 9M/6M forms, respectively. For the 9R form, the hexagonal unit cell is normalized to a "cubic" form by using the equations:

$$a_N = a/\sqrt{2}, \quad c_N = c(3\sqrt{3}), \tag{1}$$

to calculate the normalized lattice parameters for an assumed pseudo-cubic perovskite form, in which the hexagonal structure contains a sequence of six close-packed layers, with each layer consisting of the same ions of the (1 1 1) plane in the cubic structure [20]. For the 9M form, the equations are

$$a_N = a/\sqrt{6}, \quad b_N b/\sqrt{2}, \quad c_N = c \sin\beta/(2\sqrt{3}). \tag{2}$$

For the 6M form, the equations are

$$a_N = a/\sqrt{2}, \quad b_N = b/\sqrt{6}, \quad c_N = c \sin\beta/(2\sqrt{3}). \tag{3}$$

For both the 9M/9R and 6M forms, with the increasing x, a_N, b_N, c_N, and V_N are decreasing, due to the smaller ionic radius of Mn cation comparing with Ir cation [19]. For the 9M form, a_N is approximately equal to b_N at x=1/3. The value of β is also decreasing with x, which indicates the decreasing distortion degree of crystal structure.

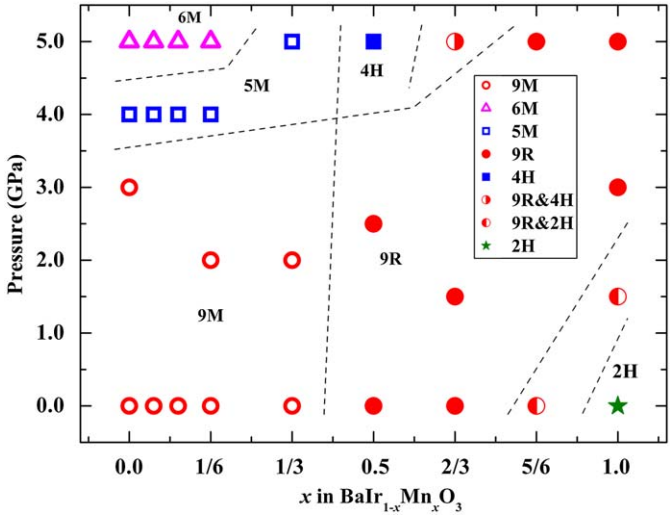

Fig. 2. Pressure–composition diagram at 1000 °C for $BaIr_{1-x}Mn_xO_3$. The dashed line is not the strict borderline between two phases.

3.2. Electrical properties

Fig. 5(a and b) shows the temperature dependences of electrical resistivity of the 9M/9R and 6M $BaIr_{1-x}Mn_xO_3$, respectively. The 9M $BaIrO_3$ is a typical semiconductor for the polycrystalline sample [9]. There is an obvious turning point in the ρ–T curve, corresponding to the Curie temperature T_c. The substitution of Mn for Ir cations in the 9M $BaIrO_3$ enhances the semiconducting property due to the localization of 3d electrons of Mn cations. Only the small doping of Mn ions (x=0.05) could result in that the kink in the ρ–T curve becomes unobvious. The ferromagnetic transition is clearly visible up to x=1/3 in the following magnetic properties, but it is not seen for $x > 0$ in Fig. 5(a). In fact, there is an unobvious turning point at the ferromagnetic transition temperature in the ρ–T curve up to x=1/6. The ferromagnetic transition temperature is decreasing with the increasing Mn content x. So the Mn substitution compresses the ferromagnetism of the 9M $BaIrO_3$. The localized 3d electrons of Mn cations tend to make the sample become insulating. The localized carriers induced by the disordered arrangement of Mn and Ir ions result in the decreasing conductance of the 9M $BaIrO_3$. The Mn doping also enhances the grain boundary effect in the sample, which may change the electrical properties of the 9M $BaIr_{1-x}Mn_xO_3$ at the ferromagnetic transition temperature. The abovementioned three factors are the possible reasons for the unobvious transition in the ρ–T curve.

The 6M $BaIrO_3$ are metals in the range of 2–300 K [6]. The substitution of Mn ions for Ir ions results in that the metallicity becomes worse. The 6M $BaIr_{1-x}Mn_xO_3$ ($x \geq 0.05$) transforms to be an insulator from a metal at higher temperature. The transition from metal to insulator at low temperature is attributed to the coexistence of the localized 3d electrons of Mn cations and itinerant electrons of Ir cations in our samples. Although the electronic itinerant of Ir cations is propitious to the metallicity of sample, the electronic localization of Mn cations tends to make the sample become insulating. The disordered arrangement of Mn and Ir ions will result in the localized carriers, which induce the sample transforms to an insulating state.

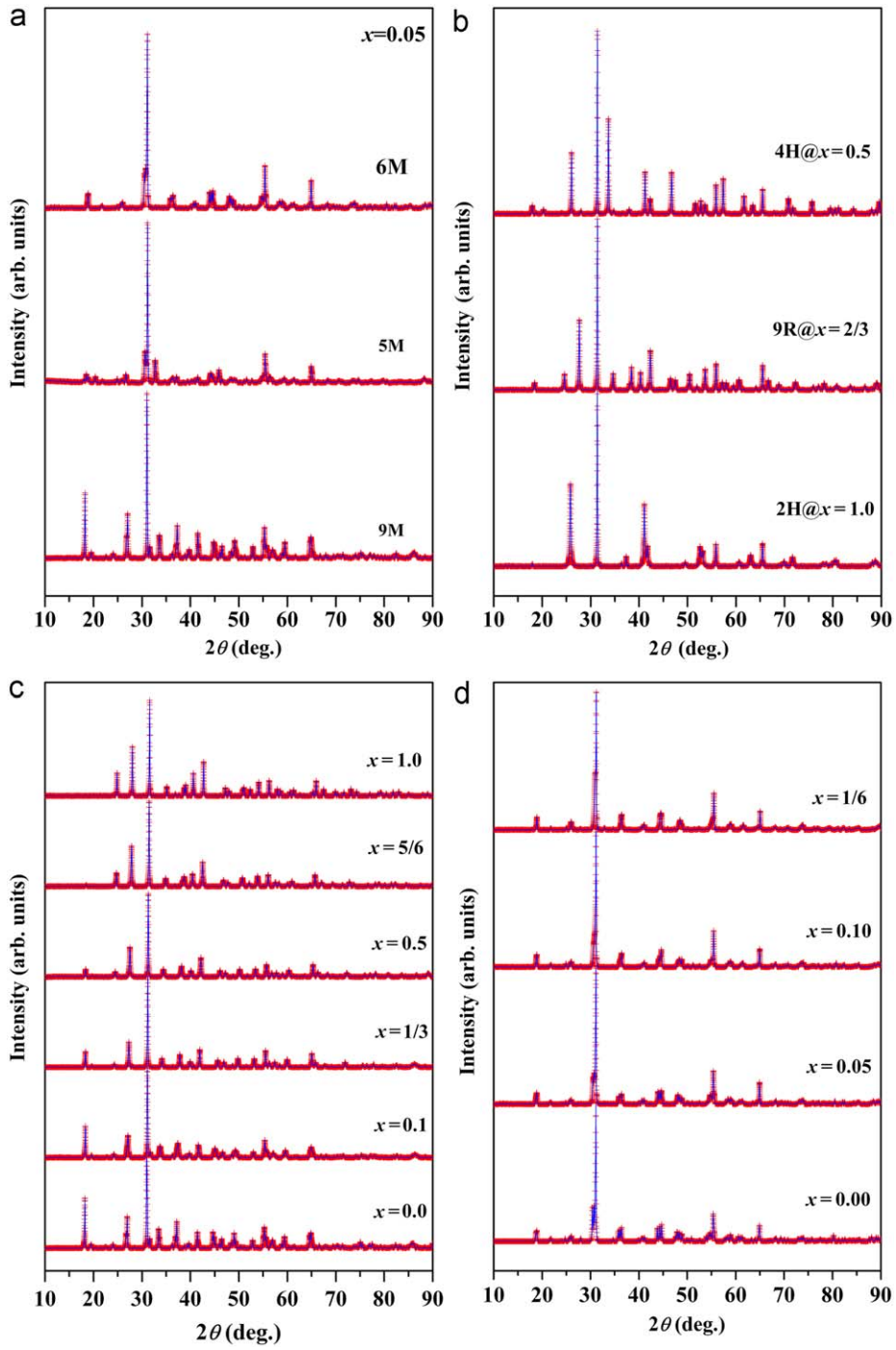

Fig. 3. The XRD patterns of $BaIr_{1-x}Mn_xO_3$: (a) the 9M, 5M, and 6M forms at $x=0.05$; (b) the 2H, 9R, and 4H forms at different x; (c) the 9M/9R forms; and (d) the 6M forms.

The inset of (b) shows the relationship of metal–insulator transition temperature T_{MI} versus x. With the increasing x, the semiconducting property is increasing. When x is equal to 1/6, the 6M form is an insulator, with the small electrical resistivity.

3.3. Magnetic properties

Fig. 6(a and b) shows the temperature dependences of magnetic susceptibility of the 9M and 9R $BaIr_{1-x}Mn_xO_3$, respectively. $BaIrO_3$ is a weak ferromagnet at low temperature, with the Curie temperature T_c is 183.8 K. The ZFC curve is same with the FC curve above T_c, but deviates from FC curve below T_c, due to the rapid zero-field cooling [21]. The Mn doping deduces the weak ferromagnetism of $BaIrO_3$. In the x range 1/3–1.0, the 9M/9R $BaIr_{1-x}Mn_xO_3$ behave spin–glass-like state at low temperature, with the glass transition temperature T_g about 60 K. The χ data at high temperature (above T_c or T_g) for the $x \leq 0.05$ samples should be fitted to the following modified Curie–Weiss law:

$$\chi = \frac{C}{T-\theta} + \chi_0, \tag{4}$$

where the parameters C, θ, and χ_0 are the Curie constant, paramagnetic Curie temperature, and the temperature

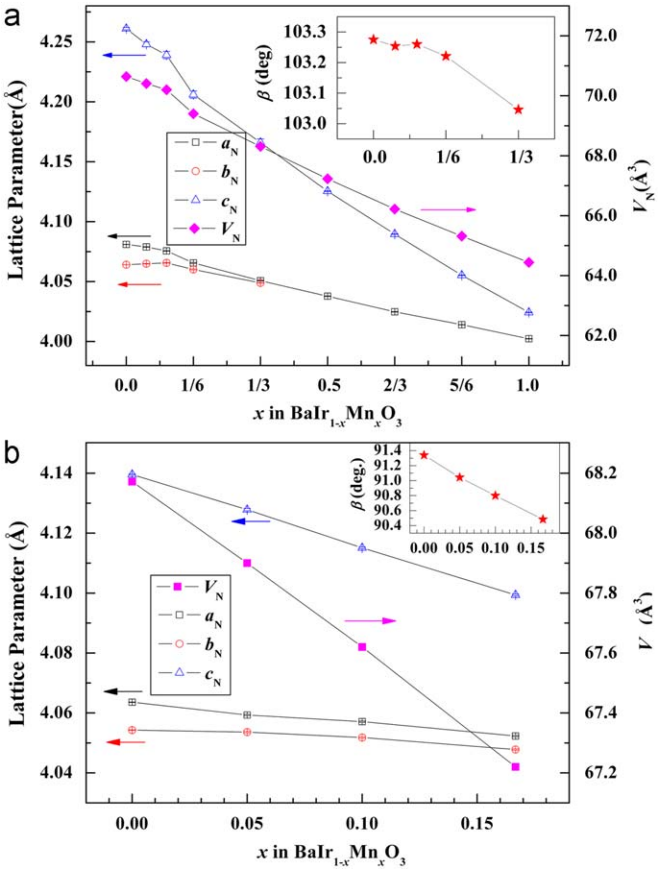

Fig. 4. The relationships of the volume of one chemical formula unit V_N versus x of $BaIr_{1-x}Mn_xO_3$: (a) the 9M/9R form; and (b) the 6M form. The insets of (a) and (b) show the relationships of β versus x for the 9M and 6M forms, respectively.

independent magnetic susceptibility, respectively. The paramagnetic effective magnetic moment μ_{eff} is obtained from the Curie constant C with the formula $\mu_{eff} = 2.828\sqrt{C}$. In the x range 0.1–2/3, the χ data at high temperature follow the Curie–Weiss law. When x is larger than 2/3, the χ–T curve at high temperature is complex, and it is difficult to fit the magnetism. The inset of Fig. 6(b) shows the relationships of effective magnetic moment μ_{eff} and paramagnetic Curie temperature θ versus x for the 9M and 9R forms at $x \le 2/3$. For the 9M/9R $BaIr_{1-x}Mn_xO_3$, μ_{eff} is smaller than the theoretic value calculated in the spin only model for the Mn and Ir cations, due to spin–orbital coupling effect and the suppressing on moments of metal cations by strong metal–metal bonding. With increasing x, μ_{eff} is increasing, which is mainly due to the enhancement of valence of cations and the superexchange interaction between Mn and Ir cations.

The paramagnetic Curie temperature θ is decreasing with the increasing x for the 9M and 9R $BaIr_{1-x}Mn_xO_3$. In the x range of 0.0–1/6, θ is positive, which indicates that the electronic spins in the two adjacent B-sites is parallel. However, when x is larger than 1/6, θ transforms to be negative, which indicates that the two adjacent electronic spins become antiparallel. The weak ferromagnetism of the 9M $BaIrO_3$ originates from spin polarization of Ir cations [3]. Mn ions doping destroys this spin polarization of Ir cations, and adds the interaction between Mn and Ir cations. The distortion degree of crystal structure is decreasing with the increasing Mn content x, which also compresses the ferromagnetism of the 9M $BaIr_{1-x}Mn_xO_3$. Therefore, with the Mn doping, these solid solutions transform to the non-ferromagnetic state, with the change from positive to negative for the paramagnetic Curie temperature θ.

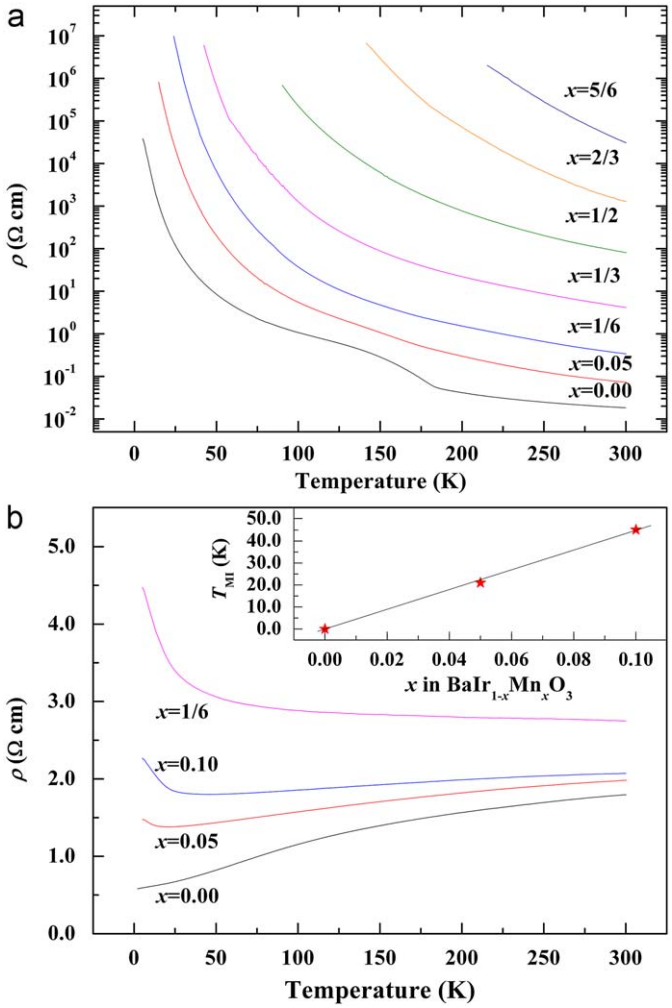

Fig. 5. Temperature dependences of electrical resistivity of $BaIr_{1-x}Mn_xO_3$: (a) the 9M/9R form; and (b) the 6M form. The inset of (b) shows the relationship of metal–insulator transition temperature T_{MI} versus x.

Fig. 6(c) shows the temperature dependences of magnetic susceptibility of the 6M $BaIr_{1-x}Mn_xO_3$. Only the ZFC curve is shown for the 6M $BaIrO_3$, because there is no obvious deviation between ZFC and FC modes. The 6M $BaIrO_3$ are paramagnetic, without the magnetic order in the experimental temperature range [6]. For the even slightly Mn doped ($x \ge 0.05$) compounds, a clear difference between ZFC and FC curves was observed. The paramagnetic susceptibility χ can be fitted to the following equation [22]:

$$\chi = \chi_{CW}(T) + \chi_{EP}(T) = \frac{C}{T-\theta} + \chi_0(1 - AT^2), \quad (5)$$

where χ_{CW} and χ_{EP} are the Curie–Weiss (CW) and exchange-enhanced Pauli (EP) contributions to magnetic susceptibility, respectively. The parameter C, θ, and χ_0 are same with those in Eq. (4). $A = (\pi^2 k_B^2/6)\{[N'(E_F)/N(E_F)]^2 - [N''E_F)/N(E_F)]\}$, where $N(E_F)$ is the density of states at Fermi level (E_F) per atom, $N'(E_F)$ and $N''(E_F)$ are its first and second energy derivatives. We attributed the temperature-independent susceptibility to the Pauli paramagnetism rather than to the spin–orbit coupling, because the 6M $BaIrO_3$ is metallic [6], with the larger electrons contribution to magnetic property, which is different from that of the insulating compounds [23]. The inset of Fig. 6(c) shows the relationships of effective magnetic moment μ_{eff} and paramagnetic Curie temperature θ versus x. Like that in the 9M/9R form, μ_{eff} of the 6M

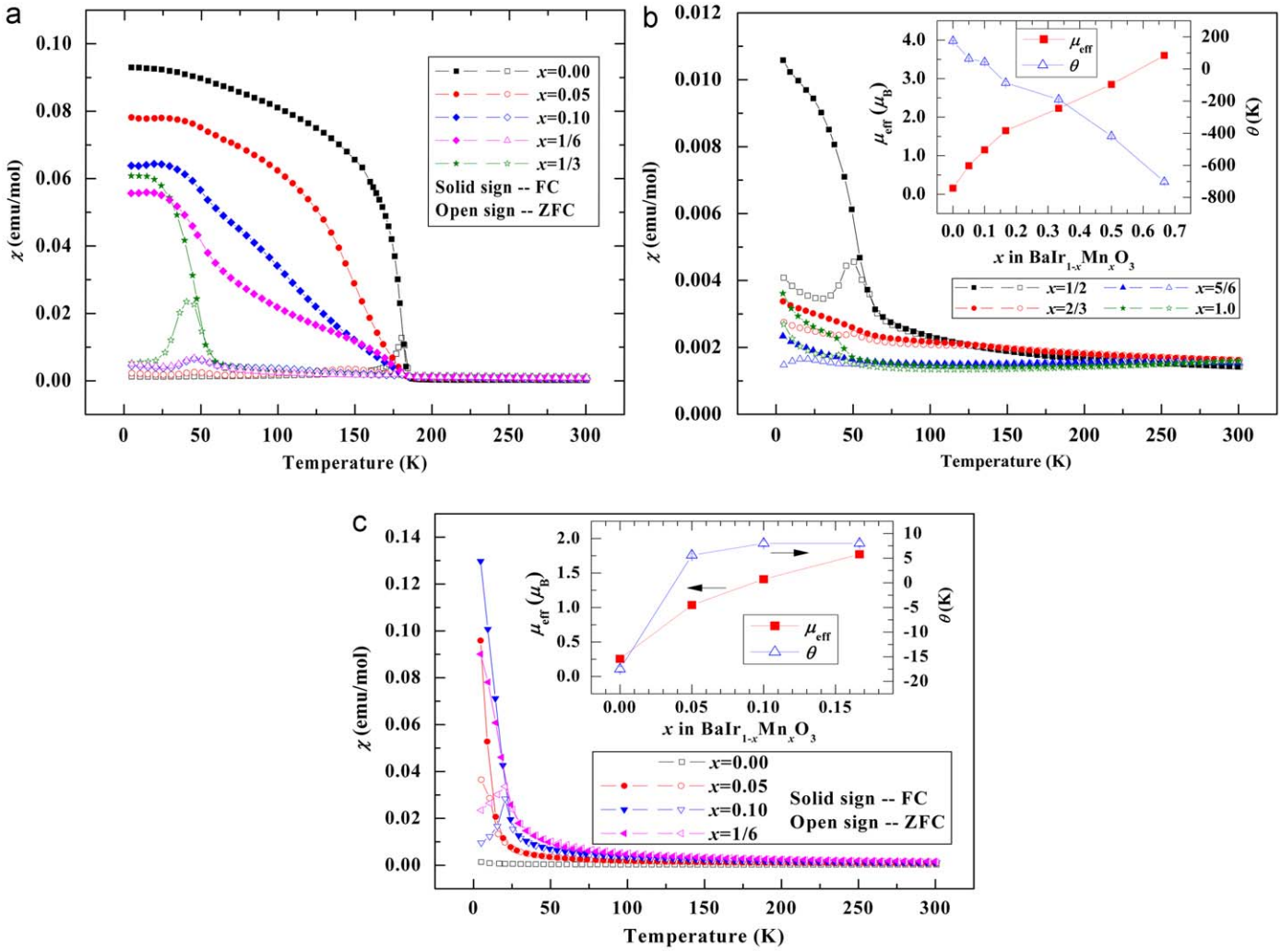

Fig. 6. Temperature dependences of magnetic susceptibility of $BaIr_{1-x}Mn_xO_3$: (a) the 9M form; (b) the 9R form; and (c) the 6M form. The insets of (b) and (c) show the relationships of effective magnetic moment μ_{eff} and paramagnetic Curie temperature θ versus x for the 9M/9R and 6M forms, respectively.

$BaIr_{1-x}Mn_xO_3$ is also smaller than the theoretic value and is increasing with the increasing x. Being different from that in the 9M/9R form, the value of θ is increasing with x and becomes positive from the original negative one for the 6M $BaIrO_3$ [6], which indicates that the electronic spins in the two adjacent B-sites transform to be parallel. The θ evolution with the increasing Mn content x for the 6M $BaIr_{1-x}Mn_xO_3$ is similar with that in the 6H $BaRu_{1-x}Mn_xO_3$ [24].

4. Conclusions

In summary, the $BaRu_{1-x}Mn_xO_3$ solid solutions were synthesized by using the solid-state chemical method and high-pressure sintering, and the XRD patterns, electrical resistivity, and magnetic susceptibility were measured. According to the XRD patterns, the pressure–composition "phase diagram" at 1000 °C of $BaIr_{1-x}Mn_xO_3$ was obtained. A systematic research about the structural, electrical, and magnetic properties evolutions of the 9M/9R and 6M $BaRu_{1-x}Mn_xO_3$ was performed. The weak ferromagnetism of the 9M/9R $BaIr_{1-x}Mn_xO_3$ is reduced by the Mn ions doping, being contrary to the semiconducting property. When the temperature is below about 60 K, these series behave spin–glass-like state at $x \geq 1/3$. The 6M $BaIrO_3$ transforms to insulator and spin–glass-like magnetism under the Mn ions substitution.

Acknowledgments

We thank Prof. C. Dong and H. Chen of Institute of Physics, Chinese Academy of Sciences for their help in XRD measurement and analysis, and the support from China Postdoctoral Science Foundation Funded Project (Grant no. 20080430932), China Postdoctoral Science Foundation Special Funded Project (Grant no. 200902410), and National Natural Science Foundation of China (Grant no. 10904022).

References

[1] T. Siegrist, B.L. Chamberland, J. Less-Common Met. 170 (1991) 93–99.
[2] R. Lindsay, W. Strange, B.L. Chamberland, R.O. Moyer Jr., Solid State Commun. 86 (1992) 759–763.
[3] G. Cao, J.E. Crow, R.P. Guertin, P.F. Henning, C.C. Homes, M. Strongin, D.N. Basov, E. Lochner, Solid State Commun. 113 (2000) 657–662.
[4] M.L. Brooks, S.J. Blundell, T. Lancaster, W. Hayes, E.L. Pratt, P.P.C. Frampton, P.D. Battle, Phys. Rev. B 71 (2005) 220411(1–4).
[5] T. Nakano, I. Terasaki, Phys. Rev. B 73 (2006) 195106(1–5).
[6] J.G. Zhao, L.X. Yang, Y. Yu, F.Y. Li, R.C. Yu, C.Q. Jin, Inorg. Chem. 48 (2009) 4290–4294.
[7] J.M. Longo, J.A. Kafalas, R.J. Arnott, J. Solid State Chem. 3 (1971) 174–179.

[8] J.G. Cheng, J.A. Alonso, E. Suard, J.S. Zhou, J.B. Goodenough, J. Am. Chem. Soc. 131 (2009) 7461–7469.
[9] N.S. Kini, A. Bentien, S. Ramakrishnan, C. Geibel, Physica B 359–361 (2005) 1264–1266.
[10] J.G. Zhao, L.X. Yang, Y. Yu, F.Y. Li, R.C. Yu, C.Q. Jin, Solid State Commun. 150 (2010) 36–39.
[11] S.-J. Kim, M.D. Smith, J. Darriet, H.-C. zur Loye, J. Solid State Chem. 177 (2004) 1493–1500.
[12] Y. Doi, Y. Hinatsu, J. Phys.: Condens. Matter 16 (2004) 2849–2860.
[13] T. Sakamoto, Y. Doi, Y. Hinatsu, J. Solid State Chem. 179 (2006) 2595–2601.
[14] T. Negas, R.S. Roth, J. Solid State Chem. 3 (1971) 323–339.
[15] E.J. Cussen, P.D. Battle, Chem. Mater. 12 (2000) 831–838.
[16] Y. Syono, S.-I. Akimoto, K. Kohn, J. Phys. Soc. Jpn. 26 (1969) 993–999.
[17] J.M. Longo, J.A. Kafalas, Mater. Res. Bull. 3 (1968) 687–692.
[18] Ch. Lang, H.K. Müller-Buschbaum, J. Less-Common Met. 157 (1990) 301–306.
[19] R.D. Shannon, Acta Crystallogr. A 32 (1976) 751–767.
[20] R.D. Burbank, H.T. Evans Jr., Acta Crystallogr. 1 (1948) 330–336.
[21] A.V. Powell, P.D. Battle, J. Alloys Compd. 191 (1993) 313–318.
[22] S.N. Kaul, A. Semwal, H.-E. Schaefer, Phys. Rev. B 62 (2000) 13892–13895.
[23] N. Segal, J.F. Vente, T.S. Bush, P.D. Battle, J. Mater. Chem. 6 (1996) 395–401.
[24] J.G. Zhao, L.X. Yang, Y. Yu, F.Y. Li, R.C. Yu, C.Q. Jin, J. Solid State Chem. 181 (2008) 1767–1775.